

Monolayer group-V binary compounds ψ -BiP and ψ -SbP with ultrahigh piezoelectricity and stability

Yuwen Zhang ^{1,2}, Tao Ouyang ^{1,2,*}, Chaoyu He ^{1,2,†}, Jin Li ^{1,2} and Chao Tang ^{1,2,‡}

¹*School of Physics and Optoelectronics, Xiangtan University, Xiangtan 411105, China*

²*Hunan Key Laboratory for Micro-nano Energy Materials and Devices, Xiangtan University, Hunan 411105, China*



(Received 27 October 2022; accepted 23 December 2022; published 17 January 2023)

Two-dimensional (2D) binary compound materials composed of group-V elements are hot spots owing to the unique easy-to-design symmetry-broken structures and excellent physical and chemical properties. In this paper, the stability and corresponding piezoelectric properties of group-V binary compounds AB ($A, B = \text{N, P, As, Sb, Bi}$, and $A \neq B$) with different structure phases are systematically investigated by performing first-principles calculations. The calculations show that the group-V binary compounds always exhibit six types of a structure phase with a relative low energy, i.e., α , β , γ , δ , λ , and ψ phases. More interestingly, compared to the obvious piezoelectric effect reported in the α phase of group-V binary compounds, a giant piezoelectric coefficient is revealed in ψ -SbP and ψ -BiP, where d_{11} is evaluated as high as 263.77 and 298.48 pm/V, respectively. Such a superb piezoelectric performance in ψ -SbP and ψ -BiP even exceeds the previously reported 2D piezoelectric material SnSe ($d_{11} = 250.58$ pm/V), which is mainly originated from a unique flexible structure and special symmetry. The mechanical, dynamical, and thermal stabilities of ψ -BiP and ψ -SbP are verified by the Born-Huang criterion, phonon spectrum, and *ab initio* molecular dynamics simulations. The findings presented in this paper shed light on the structure and piezoelectric properties of group-V binary compounds, and provide valuable guidance for their potential applications in flexible sensors and the energy harvesting community.

DOI: [10.1103/PhysRevMaterials.7.016001](https://doi.org/10.1103/PhysRevMaterials.7.016001)

I. INTRODUCTIONS

Recently, piezoelectric materials have attracted extensive attention because of their potential applications in devices requiring a conversion between electrical and mechanical energy [1–4]. The electromechanical coupling in piezoelectric materials plays critical roles in information sensing [5,6], active actuation [7,8], and nanoscale energy harvesting [7,9]. From the perspective of crystallography, two-dimensional (2D) morphology reflects the spontaneous breaking of three-dimensional symmetry. That is to say, the inversion symmetry retained in some bulk materials is broken in their corresponding 2D morphology, which might lead to inherent piezoelectricity [10]. Numerous 2D piezoelectric phenomena have also been proposed theoretically and demonstrated experimentally, e.g., Janus Pb_2SSe monolayer [11], monolayer hexagonal boron nitride [2], and transition metal dichalcogenides [12,13]. On considering the excellent mechanical strength and flexibility [14] and abundant material candidates, the investigation on 2D piezoelectric materials stimulates the sustained enthusiasm of researchers.

Black phosphorene is an emerging single-element 2D material hosted a direct band gap, high hole mobility, and unique anisotropy [15]. Analogous to black phosphorene, group-V 2D arsenene [16,17], antimonene [18–20], and bismuthene

[21,22] have also been successfully prepared experimentally, and have become new members of the 2D family. However, for one-element group-V monolayers, the structure is either centrosymmetric without intrinsic piezoelectricity or the piezoelectric coefficient is extremely tiny, which greatly limits their application in piezoelectricity [23,24]. Desynthesizing group-V monolayers into binary compounds could break the centrosymmetric structure, which might provide an effective way to improve their piezoelectric properties and thereby expand their applications in piezoelectric and flexible devices [6]. Yin *et al.* [23] conducted a systematic theoretical study on the piezoelectric effect of monolayer group-V binary compound semiconductors $A_{0.5}B_{0.5}$ ($A, B = \text{N, P, As, Sb}$, and $A \neq B$). The calculations show that the piezoelectric coefficient d_{11} of a monolayer group-V α -phase binary compound semiconductor is in the range of 6.94–243.45 pm/V, showing excellent piezoelectric performance, while the piezoelectric coefficient of the β phase is relatively much smaller, ranging from 0.67 to 4.83 pm/V. The high piezoelectric coefficient d_{11} in α -phase group-V binary compounds is as large as that of monolayer group-IV monochalcogenides, e.g., GeS ($d_{11} = 75.43$ pm/V), GeSe ($d_{11} = 212.13$ pm/V), SnS ($d_{11} = 144.76$ pm/V), and SnSe ($d_{11} = 250.58$ pm/V) [25]. Great effects have also been done in the synthesis and preparation of monolayer group-V binary compounds. Several-atomic-layer α -AsP alloys with different chemical compositions have been successfully synthesized and mechanically exfoliated, which creates the possibility of synthesizing stable group-V monolayers into binary compounds [26]. These theoretical and experimental breakthroughs indicate that monolayer group-V

*Corresponding author: ouyangtao@xtu.edu.cn

†Corresponding author: hechaoyu@xtu.edu.cn

‡Corresponding author: tang_chao@xtu.edu.cn

binary compounds are indeed an effective way to improve piezoelectric properties. It should be noted that according to the bonding features, binary alloys between group-V elements could yield remarkably rich structures in addition to the previously investigated α and β phases. Therefore, in order to fully obtain the relationship between the structure and piezoelectricity, a systematic search for the geometric structures and correctly evaluating the piezoelectric performance of monolayer group-V binary compounds is of great scientific significance and practical application value, which is quite desirable for further investigation.

Based on the above statement, in this paper, we systematically investigate the crystal structure of monolayer group-V binary compounds via a random sampling strategy combined with space group and graph theory (RG²), and their energy stability and corresponding piezoelectric properties are evaluated by means of first-principle calculations. Compared to the obvious piezoelectric effect in α -SbN ($d_{11} = 118.29$ pm/V), α -SbP ($d_{11} = 142.44$ pm/V), and α -SbAs ($d_{11} = 243.45$ pm/V), excellent piezoelectric performance is also revealed in the ψ phase of group-V binary compounds, in which the d_{11} of ψ -SbP, and ψ -BiP is evaluated as high as 263.77 and 298.48 pm/V, respectively. Such a value even exceeds the previously reported 2D piezoelectric material SnSe ($d_{11} = 250.58$ pm/V). Moreover, the mechanical, dynamical, and thermal stabilities of ψ -BiP, and ψ -SbP are confirmed as well by the Born-Huang criterion, phonon spectrum, and molecular dynamics methods.

II. COMPUTATIONAL METHODOLOGY

First-principles calculations based on density functional theory (DFT) are performed using the Vienna *ab initio* simulation package (VASP) code [27]. The generalized gradient approximation (GGA) [28] of the Perdew-Burke-Ernzerhof (PBE) functional level [29] is chosen as the exchange-correlation potential. The projector augmented-wave method is used to describe the electron-ion interactions with a plane-wave energy cutoff of 500 eV for all calculations [30]. The energy convergence criterion of electronic self-consistent field calculations is set as 10^{-7} eV. As for the geometric structure optimization, the lattice constants of 2D systems are first optimized until the forces are less than 0.01 eV/Å. Subsequently, atomic positions are optimized with fixed lattice constants until a much stricter convergence criterion of 0.001 eV/Å for the forces is reached. The Monkhorst-Pack [31] method is chosen to set the k -point meshes. The k -point grid spacing in each direction of reciprocal space is within $0.03 \times 2\pi$ Å⁻¹ generated by the VASP code [32]. Meanwhile, the thickness of the vacuum slab is set to no less than 20 Å in the z direction to avoid a mirror interaction between two neighboring monolayers. Phonon spectra are obtained using the PHONOPY package [33] with a density functional perturbation theory [34] (DFPT) approach to verify the dynamic stability. Moreover, *ab initio* molecular dynamics (AIMD) simulations are performed at temperatures of 300 K for 100 ps with a time step of 1 fs to study the thermal stability, and the Langevin thermostat approach is adopted to control temperature. The band structure is calculated using the Heyd-Scuseria-Ernzerhof (HSE06) [35] functional.

In order to obtain the elastic constant tensor C_{ij} , the energy-strain method is performed using the VASP code by fitting the total energy under seven different strain states from -1.5% to $+1.5\%$. According to Hooke's law, the elastic potential energy of a solid crystal under strain is given by [36,37]

$$\Delta E = \frac{V}{2} \sum_{i=1}^6 \sum_{j=1}^6 C_{ij} \varepsilon_i \varepsilon_j \quad (1)$$

where V is the volume of a lattice cell without distortion, ΔE is the energy increment from the strain with vector $\varepsilon = (\varepsilon_1, \varepsilon_2, \varepsilon_3, \varepsilon_4, \varepsilon_5, \varepsilon_6)$, and C_{ij} is the element of the elastic constant C matrix. Based on the assumption that a 2D system does not have a particular thickness, the unit for stress and elastic moduli is force per unit length (N m^{-1}) rather than force per unit area (N m^{-2}). Thus, volume V is reduced to area A_0 of the undistorted 2D lattice cell. Accordingly, one can obtain the relationship between ΔE and ε when applying a specific strain ε .

On the other hand, DFPT [34] and the modern theory of polarization based on Berry's phase approximation are [38,39] used to calculate the piezoelectric stress coefficient e_{ij} . The relaxed-ion elastic and piezoelectric tensors are obtained as the sum of ionic and electronic contributions [12],

$$C_{ijkl} = \frac{d\sigma_{ij}}{d\varepsilon_{kl}} = C_{ijkl}^{\text{ion}} + C_{ijkl}^{\text{el}}, \quad (2)$$

$$e_{ijk} = \frac{dP_i}{d\varepsilon_{jk}} = e_{ijl}^{\text{ion}} + e_{ijl}^{\text{el}}, \quad (3)$$

$$d_{ijk} = \frac{dP_i}{d\sigma_{jk}}, \quad (4)$$

where σ_{jk} , ε_{jk} , and P_i are the stress tensor, strain tensor, and polarization, respectively. The polarization components of the polarization tensor P_i along the x , y , and z directions are indicated by the subscripts $i = 1, 2, 3$, respectively. By applying Voigt notation, the 2D elastic and piezoelectric tensors are transformed as [12,40]

$$C_{ij} = \begin{pmatrix} C_{11} & C_{12} & C_{16} \\ C_{21} & C_{22} & C_{26} \\ C_{61} & C_{62} & C_{66} \end{pmatrix}, \quad (5)$$

$$e_{ij} = \begin{pmatrix} e_{11} & e_{12} & e_{16} \\ e_{21} & e_{22} & e_{26} \\ e_{31} & e_{32} & e_{36} \end{pmatrix}, \quad (6)$$

$$d_{ij} = \begin{pmatrix} d_{11} & d_{12} & d_{16} \\ d_{21} & d_{22} & d_{26} \\ d_{31} & d_{32} & d_{36} \end{pmatrix}. \quad (7)$$

Here, the d_{ij} tensor is used to describe the responding strain induced by applying the electric field, and the e tensor represents the responding polarization induced by the applying strain. Finally, the strain coefficients of the piezoelectric tensor, which are essential for piezoelectric applications, could be evaluated,

$$e_{ik} = d_{ij} C_{jk}. \quad (8)$$

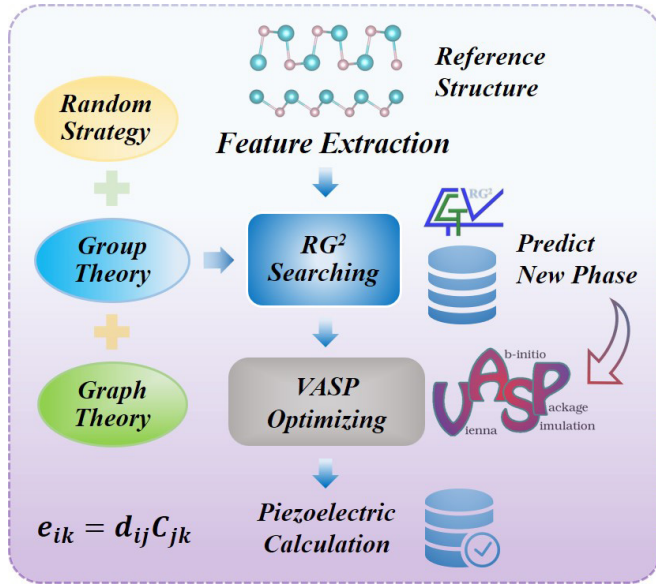


FIG. 1. Combination of RG^2 and VASP for piezoelectric materials design.

III. RESULTS AND DISCUSSION

A. Allotrope and binding energy

The crystal structure is the starting point of the simulation calculation and could provide useful guidance for synthesizing in experiment. In this paper, different from traditional artificial structural modifications, the crystal structure of monolayer group-V binary compounds $A_{0.5}B_{0.5}$ ($A, B = N, P, As, Sb, Bi$, and $A \neq B$) is systematically searched based on a random sampling strategy combined with space group and graph theory as performed in the RG^2 code [45]. Figure 1 illustrates the detailed search process used to construct the structural phase diagram. Here, the known α and β phases are utilized as reference structures. The conjugate gradient algorithm is adopted to optimize the searched monolayer group-V binary structures. On considering the uniqueness of the piezoelectric structure, six typical crystals of monolayer group-V binary compounds, with potentially high piezoelectric coefficients, are chosen as the main study objectives. As shown in Fig. 2, among six typical crystals, the γ , α , δ , ψ , and λ phases are an orthorhombic system, and the β phase is a hexagonal system. Accordingly, to facilitate the calculations of elastic and piezoelectric properties, an orthorhombic supercell including four atoms is constructed for the β phase.

In order to evaluate the energy stability of the monolayer group-V binary compounds, the binding energy is calculated by using the following equation [46],

$$E_b = (E_{\text{total}} - nE_A - mE_B)/(n + m), \quad (9)$$

where E_{total} denotes the total energies of these monolayer compounds, and E_A and E_B represent the energy of the isolated atom of A and B in a large enough box, respectively. n and m are the numbers of A and B atoms in the unit cell. Taking BiP and SbP binary allotrope compounds as an example, the total energies per atom are depicted in Fig. 3. It can be found that the six typical phases always exhibit a relatively low energy.

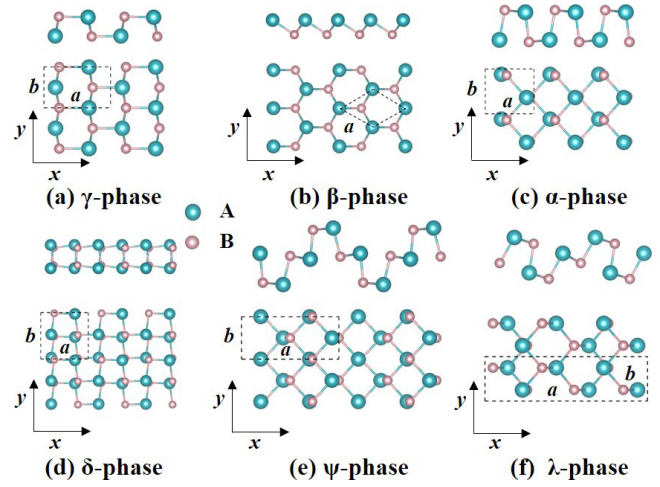


FIG. 2. Schematic diagram of the monolayer group-V binary compounds with α -, γ -, δ -, and ψ -phase structures with $mm2$ point-group symmetry, λ -phase structures with m point-group symmetry, and β -phase structures with $3m$ point-group symmetry. ($A, B = N, P, As, Sb, Bi$, and $A \neq B$.)

For BiP and SbP, the α phase possesses the lowest binding energy, while β -BiP and γ -SbP have the highest binding energy among the six typical phases. The energy difference between β -BiP and α -BiP is only 0.061 eV/atom and that between γ -SbP and α -SbP is merely 0.042 eV/atom. The energy data of PN, AsN, SbN, BiN, AsP, SbAs, BiAs, and BiSb are provided in the Supplemental Material (Fig. S1) [47]. These binding energy results confirm the rationality and scientificity of our selection on the six typical phases.

B. Piezoelectricity and electronic properties

To determine the piezoelectric strain tensor, the elastic stiffness coefficients C_{11} , C_{22} , and C_{12} of the γ -, β -, α -, δ -, ψ -, and λ -phase compounds are calculated first by using the energy-strain method. Similar to the experimental treatment we calculate the elastic constant of the material using the “relaxed-ion” method [13], i.e., the atoms are relaxed with a fixed lattice constant (or fixed strain), and then the energy-strain parabolic fitting is performed to obtain the elastic stiffness coefficients. Table I summarizes the relaxed-ion elastic stiffness coefficients C_{11} , C_{22} , and C_{12} of the monolayer group-V binary compounds. As shown in Table I, for some of the reported materials, our calculation results are in good agreement with previous calculation results in the literature

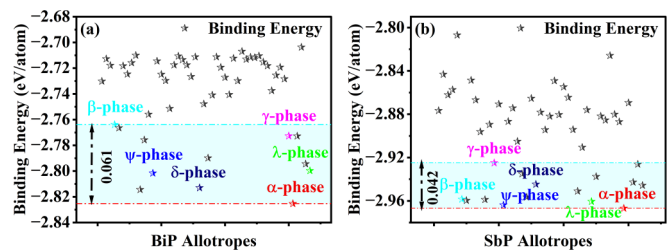


FIG. 3. The total energies per atom of BiP and SbP binary allotrope compounds.

TABLE I. Lattice parameters and relaxed-ion elastic stiffness coefficients C_{11} , C_{22} , and C_{12} of α -, β -, γ -, δ -, ψ -, and λ -phase group-V binary compounds calculated at the DFT-PBE level. C_{11} , C_{22} , and C_{12} are in units of N/m.

Material	a (Å)	b (Å)	C_{11}	C_{22}	C_{12}
α -PN	4.16, 4.16 [23]	2.67, 2.70 [23]	44.37, 43.30 [23]	207.95, 204.10 [23]	25.43, 24.40 [23]
β -PN	2.72, 2.73 [23]		151.55, 150.20 [23]	151.62	20.50
δ -PN	4.50, 4.51 [36]	5.04, 5.05 [36]	135.23	53.93	-4.93
λ -PN	11.87	2.69	31.98	198.17	5.91
α -AsN	4.18, 4.18 [23]	2.96, 2.96 [23]	19.90, 20.60 [23]	145.14, 144.30 [23]	17.79, 17.80 [23]
β -AsN	2.97, 2.97 [23]		106.45, 105.80 [23]	106.52	23.22
γ -AsN	4.73	3.00	38.60	95.71	10.50
δ -AsN	4.80, 4.80 [36]	5.24, 5.24 [36]	83.20	32.23	-5.73
λ -AsN	13.03	2.97	23.88	133.25	15.51
α -SbN	4.16, 4.19 [23]	3.30, 3.30 [23]	8.81, 7.80 [23]	107.50, 107.30 [23]	12.25, 13.00 [23]
β -SbN	3.27, 3.27 [23]		80.60, 80.60 [23]	80.62	20.88
γ -SbN	4.29, 4.28 [41]	3.42, 3.42 [41]	79.78, 77.15 [41]	72.22, 72.22 [41]	57.64, 42.84 [41]
δ -SbN	5.16, 5.18 [36]	5.61, 5.64 [36]	42.62	22.05	-6.57
λ -SbN	14.05	3.28	20.08	89.59	3.89
α -BiN	3.75, 3.79 [36]	3.52, 3.53 [36]	27.62	96.3	7.22
β -BiN	3.47	3.47	57.14	57.24	15.56
γ -BiN	4.53	3.58	59.07	59.69	33.61
δ -BiN	5.24, 5.27 [36]	5.52, 5.60 [36]	30.05	14.71	-1.07
ψ -BiN	6.95	3.52	21.17	89.06	7.96
λ -BiN	12.58	3.53	21.43	80.06	13.25
α -AsP	4.69, 4.69 [23]	3.50, 3.50 [23]	18.99	79.8	18.87
β -AsP	3.45, 3.46 [23]		63.55, 62.90 [23]	63.73	9.64
γ -AsP	5.65, 5.66 [41]	3.44, 3.44 [41]	47.77, 48.28 [41]	70.63, 69.48 [41]	-1.81, -1.58 [41]
δ -AsP	5.66, 5.66 [42]	5.70, 5.71 [42]	61.02	31.44	-10.29
ψ -AsP	9.41	3.48	9.86	78.74	10.66
λ -AsP	14.59	3.49	17.8	76.37	14.85
α -SbP	4.39, 4.43 [23]	3.92, 3.91 [23]	12.03	61.23	13.91
β -SbP	3.73, 3.73 [23]		48.42, 46.80 [23]	48.55	8.95
γ -SbP	5.95, 5.96 [41]	3.72, 3.72 [41]	26.36, 28.07 [41]	53.24, 53.75 [41]	1.46, 1.68 [41]
δ -SbP	5.88	5.77	47.45	24.54	-18.16
ψ -SbP	9.03	3.83	4.00	61.32	9.90
λ -SbP	14.95	3.81	12.44	59.04	16.07
α -BiP	4.46, 4.33 [42], 4.69 [43]	4.10, 4.15 [42], 4.10 [43]	13.5	48.72	11.23
β -BiP	3.88		39.73	39.86	9.00
γ -BiP	6.10, 6.11 [41]	3.87, 3.87 [41]	25.81, 26.78 [41]	43.00, 42.40 [41]	0.59, 0.02 [41]
ψ -BiP	8.42	4.00	3.16	53.94	2.84
λ -BiP	14.64	4.02	18.93	51.65	16.55
α -SbAs	4.65, 4.73 [23], 4.60 [43]	4.04, 4.04 [23], 4.05 [43]	6.56, 8.80 [23]	49.24, 49.9 [23]	8.98, 14.60 [23]
β -SbAs	3.86, 3.87 [23]		41.24, 40.8 [23]	41.44	8.09
γ -SbAs	6.26, 6.24 [41]	3.85, 3.85 [41]	39.61, 23.13 [41]	46.14, 29.34 [41]	-0.05, -1.60 [41]
δ -SbAs	6.20, 6.21 [42]	6.14, 6.12 [42]	36.62	27.87	-14.35
ψ -SbAs	9.70	3.94	6.59	54.12	11.00
λ -SbAs	15.34	3.95	13.26	50.72	15.3
α -BiAs	4.61, 4.60 [42]	4.23, 4.24 [42]	19.3	53.02	16.43
β -BiAs	4.00, 4.00 [42]		35.11	34.77	8.06
γ -BiAs	6.40	3.98	33.07	38.35	-0.03
ψ -BiAs	9.44	4.11	8.43	49.3	9.12
λ -BiAs	15.20	4.13	16.73	45.77	15.3
α -BiSb	4.77, 4.81 [42]	4.49, 4.46 [42]	18.77	43.92	12.01
β -BiSb	4.23, 4.24 [42]		27.9	28.21	6.31
γ -BiSb	6.79	4.21	20.8	32.23	-0.12
ψ -BiSb	10.01	4.35	6.16	40.26	7.16
λ -BiSb	16.07	4.37	14.5	37.69	12.77

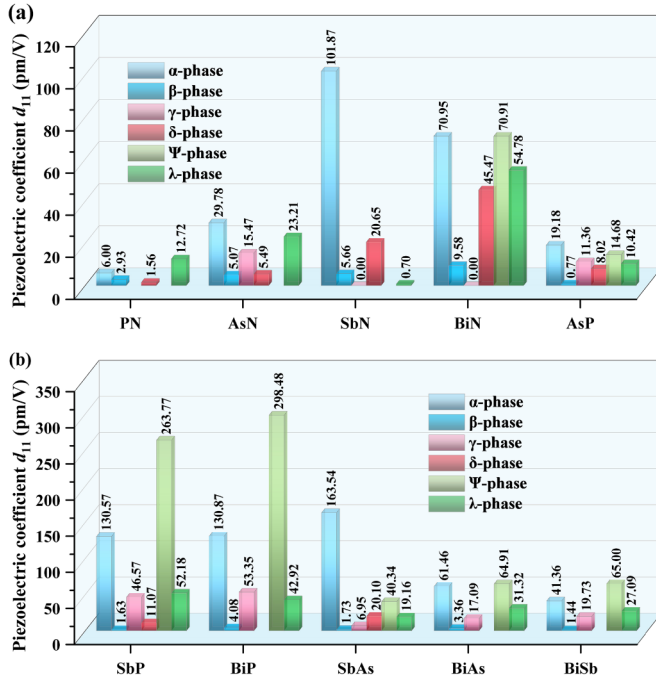


FIG. 4. Relaxed-ion piezoelectric coefficients d_{11} for α -, β -, γ -, δ -, ψ -, and λ -phase monolayers of group-V binary compounds.

[23,36,41–43], which ensures the reliability and scientificity of our calculations. Meanwhile, one can note that all monolayer group-V binary compounds with six typical phases, except for γ -PN, ψ -PN, ψ -AsN, ψ -SbN, δ -BiP, δ -BiAs, and δ -BiSb, satisfy the Born-Huang criteria [32,48], where $C_{11} > 0$, $C_{66} > 0$, and $C_{11} * C_{22} > C_{12}^2$, endowing the mechanical stability of them. Among the six phases studied in this paper, the λ , α , and ψ phases of monolayer group-V binary compounds tend to have the lower elastic stiffness coefficients C_{11} . In contrast, except for BiN, the elastic stiffness coefficient C_{11} of the β phase is the highest among the six phases. Such behavior could be understood from their discrepancies of structure. The ψ phase can be considered as a mirror image inversion of one of the two adjacent unit cells of the α phase in the z direction, and the λ phase can be viewed as an alternating combination of the α phase and the β phase. That is to

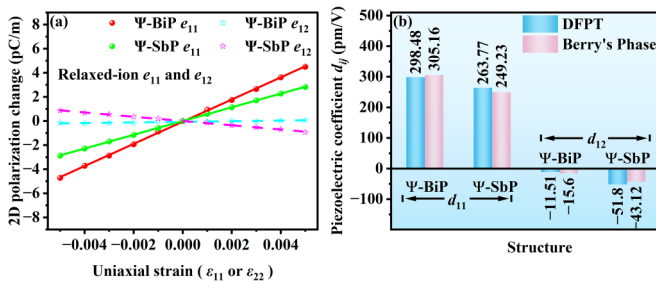


FIG. 5. (a) Calculated polarization changes per area along the x direction under the applied uniaxial strain ϵ_{11} along the x direction and ϵ_{22} along the y direction for ψ -BiP and ψ -SbP monolayers. (b) Relaxed-ion piezoelectric coefficients d_{11} and d_{12} for ψ -BiP and ψ -SbP monolayers by DFPT and Berry's phase methods, respectively.

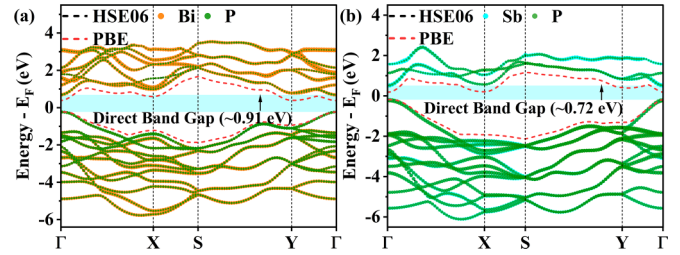


FIG. 6. Calculated electronic band structures PBE and HSE06 for monolayer binary compounds (a) ψ -BiP and (b) ψ -SbP. For graphical clarity, the PBE only shows the valence-band maximum (VBM) and conduction-band minimum (CBM).

say, the λ , α , and ψ phases hold flexible puckered structures [23], which might lead to lower elastic stiffness coefficients C_{11} . As for the β phase, its larger C_{11} could be explained by the honeycomblike phase structure. Moreover, the quite small elastic stiffnesses C_{11} of ψ -SbP (4.00 N/m) and ψ -BiP (3.16 N/m) imply that a giant piezoelectric coefficient d_{11} might appear in the x direction, according to the definition of Eq. (8).

In order to obtain the piezoelectric coefficient d_{ij} , the e_{ij} coefficient must be evaluated first based on the DFPT [34] method as implemented in the VASP code [27]. After that, the piezoelectric coefficients d_{11} and d_{12} , important indicators of electromechanical energy conversion efficiency, can be calculated based on Eqs. (4)–(7). A summary of the relaxed-ion piezoelectric coefficients e_{11} , e_{12} , d_{11} , and d_{12} of the monolayer structures of PN, AsN, SbN, BiN, AsP, SbP, BiP, SbAs, BiAs, and BiSb with the γ , β , α , δ , ψ , and λ phases are presented in Table II. One can find that for some reported materials, our calculation results are in good agreement with previous literature [23]. However, for α -SbP, our calculation results are only 163.5 pm/V, while 243.45 pm/V was reported by Yin *et al.* [23]. This discrepancy might be attributed to the difference in structure optimization accuracy and calculation method, which has also been found in the previous literature [1,25,49]. In recent years, 2D materials that exhibit a large piezoelectric response have attracted tremendous attention. Besides the most studied h -BN and MoS₂, Fei *et al.* reported that the monolayer group-IV monochalcogenides also present an excellent piezoelectric performance, e.g., SnSe ($d_{11} = 250.58$ pm/V) and GeSe ($d_{11} = 212.13$ pm/V) [25]. Interestingly, as shown in Table II and Fig. 4, the relaxed-ion coefficients d_{11} of ψ -SbP and ψ -BiP are 263.77 and 298.48 pm/V, respectively. Such values exceed the previously reported α -phase binary compounds with piezoelectric coefficients ranging from 6.94 to 243.45 pm/V [23], as well as group-IV monochalcogenides SnSe [25] and GeSe [25], confirming the excellent piezoelectric performance of ψ -SbP and ψ -BiP. As for other binary monolayers, e.g., α -BiN, α -BiP, α -BiAs, α -BiSb, ψ -BiAs, and ψ -BiSb, they exhibit relatively modest relaxed-ion piezoelectric coefficients d_{11} of 70.95, 130.87, 61.46, 41.36, 64.91, and 65.00 pm/V, respectively. Nevertheless, their coefficients are still much larger than those of $2H$ -MoS₂ ($d_{11} = 3.73$ pm/V), and $2H$ -MoSe₂ and $2H$ -MoTe₂ ($d_{11} = 9.13$ pm/V) [13].

TABLE II. DFT-PBE calculated relaxed-ion piezoelectric coefficients (e_{11} , e_{12} , d_{11} , and d_{12}), band gaps (E_g , direct \uparrow , indirect \nearrow), and point group and space group for α -, β -, γ -, δ -, ψ -, and λ -phase monolayers of group-V binary compounds. The e_{11} and e_{12} are in units of 10^{-10} C/m, d_{11} , d_{12} are in units of pm/V, and E_g are in units of eV.

Material	e_{11}	e_{12}	d_{11}	d_{12}	E_g	Point group	Space group
α -PN	2.08, 2.41 [23]	-3.27, -3.28 [23]	6.00, 6.94 [23]	-2.31, -2.44 [23]	1.66, 2.18 [23], 1.64 [44] \nearrow	$mm2$	$Pmn2_1$
β -PN	3.85, 3.60 [23]		2.93, 2.77 [23]		1.81, 1.81 [23] \nearrow	$3m$	$P3m1$
δ -PN	1.81	3.21	1.56	6.11	2.22, 2.25 [36] \nearrow	$mm2$	$Pca2_1$
λ -PN	4.24	6.78	12.72	3.05	1.92 \nearrow	m	Cm
α -AsN	4.85, 4.98 [23]	-3.45, -3.11 [23]	29.78, 29.14 [23]	-6.03, -2.44 [23]	1.9, 1.91 [23] \nearrow	$mm2$	$Pmn2_1$
β -AsN	4.22, 4.00 [23]		5.07, 4.83 [23]		1.97, 1.98 [23] \nearrow	$3m$	$P3m1$
γ -AsN	6.54	6.81	15.46	5.42	1.41 \nearrow	$mm2$	$Pmn2_1$
δ -AsN	3.93	3.29	5.49	11.17	2.00, 2.11 [36] \uparrow	$mm2$	$Pca2_1$
λ -AsN	4.7	-3.68	23.21	-5.46	1.71 \nearrow	m	Cm
α -SbN	7.57, 7.51 [23]	0.13, 1.21 [23]	101.87, 118.29 [23]	-11.49, -13.20 [23]	1.77, 1.90 [23], 1.82 [15] \nearrow	$mm2$	$Pmn2_1$
β -SbN	3.38, 3.16 [23]		5.66, 5.30 [23]		1.67, 1.68 [23] \nearrow	$3m$	$P3m1$
γ -SbN	0.00	0.00	0.00	0.00	1.15 \nearrow	mmm	$Pmmn$
δ -SbN	7.55	2.83	20.65	18.96	2.02, 2.33 [36] \uparrow	$mm2$	$Pca2_1$
λ -SbN	0.37	5.24	0.7	5.82	1.84 \nearrow	m	Cm
α -BiN	19.49	3.65	70.95	-1.52	1.46, 1.46 [36] \nearrow	$mm2$	$Pmn2_1$
β -BiN	3.98		9.58	5.45	0.75 \nearrow	$3m$	$P3m1$
γ -BiN	0.00	0.00	0.00	0.00	0.73 \nearrow	mmm	$Pmmn$
δ -BiN	13.4	3.11	45.47	24.43	1.68, 1.70 [36] \uparrow	$mm2$	$Pca2_1$
ψ -BiN	14.53	3.04	70.91	-5.99	1.11 \nearrow	$mm2$	$Pmc2_1$
λ -BiN	10.46	-0.47	54.78	-9.66	1.07 \uparrow	m	Cm
α -AsP	2.69, 2.68 [23]	-0.46, -0.25 [23]	19.18, 18.90 [23]	-5.11, -4.74 [23]	0.91, 0.90 [23] \uparrow	$mm2$	$Pmn2_1$
β -AsP	0.41, 0.36 [23]		0.77, 0.67 [23]		1.84, 1.86 [23] \nearrow	$3m$	$P3m1$
γ -AsP	5.41, 9.72 [41]	0.37, 0.58 [41]	11.36, 20.17 [41]	0.81, 1.30 [41]	0.76 \nearrow	$mm2$	$Pmn2_1$
δ -AsP	4.42	0.63	8.02	4.63	0.77, 0.79 [42] \nearrow	$mm2$	$Pca2_1$
ψ -AsP	1.15	-0.59	14.65	-2.73	1.08 \uparrow	$mm2$	$Pmc2_1$
λ -AsP	1.43	-0.64	10.42	-2.85	1.00 \uparrow	m	Cm
α -SbP	11.51, 11.00 [23]	-0.29, 2.02 [23]	130.57, 142.44 [23]	-30.15, -27.64 [23]	0.52, 0.71 [23] \nearrow	$mm2$	$Pmn2_1$
β -SbP	0.93, 0.86 [23]		1.63, 1.65 [23]		1.73, 1.75 [23] \nearrow	$3m$	$P3m1$
γ -SbP	12.28, 15.25 [41]	0.91, 1.06 [41]	46.57, 54.33 [41]	0.42, 0.28 [41]	0.82 \nearrow	$mm2$	$Pmn2_1$
δ -SbP	4.63	-1.17	11.07	3.43	0.74 \nearrow	$mm2$	$Pca2_1$
ψ -SbP	5.99	-2.03	263.77	-45.9	0.37 \uparrow	$mm2$	$Pmc2_1$
λ -SbP	3.81	-1.48	52.18	-16.71	0.75 \uparrow	m	Cm
α -BiP	14.76	2.09	130.87	-25.86	0.57, 0.58 [43] \nearrow	$mm2$	$Pmn2_1$
β -BiP	1.26		4.08		1.45 \uparrow	$3m$	$P3m1$
γ -BiP	13.80, 17.24 [41]	2.89, 2.87 [41]	53.35, 64.35 [41]	5.99, 6.74 [41]	0.77 \nearrow	$mm2$	$Pmn2_1$
ψ -BiP	9.00	0.26	298.48	-15.22	0.62 \uparrow	$mm2$	$Pmc2_1$
λ -BiP	5.07	-2.43	42.92	-18.46	0.48 \uparrow	m	Cm
α -SbAs	8.48, 12.13 [23]	2.35, 3.78 [23]	163.54, 243.45 [23]	-25.03, -63.65 [23]	0.23, 0.29 [23] \uparrow	$mm2$	$Pmn2_1$
β -SbAs	0.58, 0.54 [23]		1.73, 1.65 [23]		1.47, 1.49 [23] \nearrow	$3m$	$P3m1$
γ -SbAs	2.75, 6.40 [41]	0.72, 1.13 [41]	6.95, 28.05 [41]	1.57, 5.38 [41]	0.83 \uparrow	$mm2$	$Pmn2_1$
δ -SbAs	2.68	6.15	20.01	32.37	0.62, 0.57 [42] \nearrow	$mm2$	$Pca2_1$
ψ -SbAs	1.63	-0.63	40.34	-9.37	0.34 \uparrow	$mm2$	$Pmc2_1$
λ -SbAs	1.36	-0.98	19.16	-7.72	0.56 \uparrow	m	Cm
α -BiAs	-7.93	2.59	61.46	-23.94	0.54, 0.54 [42] \uparrow	$mm2$	$Pmn2_1$
β -BiAs	0.9		3.36		1.06, 1.08 [42] \uparrow	$3m$	$P3m1$
γ -BiAs	5.65	2.09	17.09	5.46	0.75 \nearrow	$mm2$	$Pmn2_1$
ψ -BiAs	4.25	-0.72	64.91	-13.47	0.31 \uparrow	$mm2$	$Pmc2_1$
λ -BiAs	2.83	-2.41	31.32	-15.73	0.36 \uparrow	m	Cm
α -BiSb	6.02	-1.38	41.36	-14.47	0.52, 0.44 [42], 0.46 [43] \uparrow	$mm2$	$Pmn2_1$
β -BiSb	0.31		1.44		0.96, 0.98 [42] \uparrow	$3m$	$P3m1$
γ -BiSb	4.10	0.54	19.73	1.75	0.68 \uparrow	$mm2$	$Pmn2_1$
ψ -BiSb	3.21	18.46	65	-11.1	0.34 \uparrow	$mm2$	$Pmc2_1$
λ -BiSb	2.55	-0.6	27.09	-10.78	0.32 \uparrow	m	Cm

TABLE III. Relaxed-ion piezoelectric coefficients (e_{11} , e_{12} , d_{11} , and d_{12}) for ψ -BiP and ψ -SbP monolayers by DFPT and Berry's phase methods, respectively. The e_{11} and e_{12} are in units of 10^{-10} C/m, and d_{11} , d_{12} are in units of pm/V.

Materials	DFPT				Berry's phase			
	e_{11}	e_{12}	d_{11}	d_{12}	e_{11}	e_{12}	d_{11}	d_{12}
ψ -BiP	9.00	0.26	298.84	-11.51	9.20	0.25	305.16	-15.60
ψ -SbP	5.99	-2.03	263.77	-51.8	5.70	-1.77	249.23	-43.12

Following this result, according to the definition of the piezoelectric tensors e_{ij} in Eq. (3), the e_{ij} coefficients of ψ -SbP and ψ -BiP are further verified by using the Berry's phase method [38,39]. For ψ -BiP and ψ -SbP with $mm2$ point-group symmetry, the independent piezoelectric coefficients e_{11} , e_{12} , e_{26} , d_{11} , d_{12} , and d_{26} are nonzero [23]. The coefficients e_{26} and d_{26} represent the piezoelectric effect of polarization along the y direction subjected to an applied shear strain on the xy plane. Here, we specifically pay attention to the coefficients e_{11} , e_{21} , d_{11} , and d_{12} . Based on Eq. (8), we can obtain d_{11} and d_{12} from e_{11} , e_{12} , C_{11} , C_{22} , and C_{12} as [23,25]

$$\begin{aligned} d_{11} &= \frac{e_{11}C_{22} - e_{12}C_{12}}{C_{11}C_{22} - C_{12}^2}, \\ d_{12} &= \frac{e_{12}C_{11} - e_{11}C_{12}}{C_{11}C_{22} - C_{12}^2}. \end{aligned} \quad (10)$$

The calculated results obtained from the Berry's phase method are shown in Fig. 5 and Table III summarizes the relaxed-ion elastic stiffness coefficients e_{11} , e_{12} , d_{11} , and d_{12} of ψ -BiP and ψ -SbP. The DFPT results are provided in Table III for comparison. Figure 5(a) illustrates the linear relationship between polarization changes and strains for ψ -BiP and ψ -SbP monolayers in the range of uniaxial strain -0.5% to 0.5% . From Fig. 5(b) one can find that the piezoelectric coefficients d_{11} and d_{12} calculated with the DFPT are in excellent agreement with those calculated with Berry's phase approximation. This result further confirms that ψ -BiP and ψ -SbP host superb piezoelectric coefficients. Meanwhile, it is found that the piezoelectric effect in the ψ -BiP and ψ -SbP monolayers is extremely anisotropic, where d_{11} is one order of magnitude greater than d_{12} . These anisotropic behaviors may be useful in designing nanosized sensors and energy harvesting devices with particular demands.

The band gap and band-gap characteristics of materials also play an important role in determining the applications. At the DFT-PBE level, 25 of the group-V binary allotropes

of the α , β , γ , δ , λ , and ψ phases belong to direct band-gap semiconductors, 28 to indirect band-gap semiconductors, and the remaining 7 either undergo a structural phase transition after optimization or are elastically unstable. Their band gaps range from 0.23 to 2.22 eV. As we know, PBE functionals usually underestimate the band gap of materials. More accurate band-gap values can be obtained by the *GW* [50] method or hybrid functionals such as HSE06 [35,51]. We calculate the band structure of ψ -BiP and ψ -SbP using HSE06 as well. It can be seen from Fig. 6 that ψ -BiP and ψ -SbP exhibit direct band-gap semiconductors, and their gap values are 0.91 and 0.72 eV, respectively.

C. Mechanical, dynamical, and thermal stability

Finally, for ensuring the reliability of applications, we investigate the lattice's dynamic, thermal, and mechanical stabilities of ψ -BiP and ψ -SbP. For monolayer materials with orthogonal crystal systems, there are four independent elastic constants [32], C_{11} , C_{12} , C_{22} , and C_{66} :

$$C_{ij} = \begin{pmatrix} C_{11} & C_{12} & 0 \\ C_{12} & C_{22} & 0 \\ 0 & 0 & C_{66} \end{pmatrix}. \quad (11)$$

It is obvious that the elastic constants satisfy the Born-Huang criteria [32,48], $C_{11} > 0$, $C_{66} > 0$, and $C_{11} * C_{22} > C_{12}^2$, demonstrating the mechanical stability of ψ -BiP and ψ -SbP. In this paper, the orientation-dependent elastic constants are also calculated by using the following equations [37,52],

$$Y(\theta) = \frac{(C_{11}C_{22} - C_{12}^2)}{C_{22} \cos^4(\theta) + A \cos^2(\theta) \sin^2(\theta) + C_{11} \sin^4(\theta)}, \quad (12)$$

$$\nu(\theta) = \frac{C_{12} \cos^4(\theta) - B \cos^2(\theta) \sin^2(\theta) + C_{12} \sin^4(\theta)}{C_{22} \cos^4(\theta) + A \cos^2(\theta) \sin^2(\theta) + C_{11} \sin^4(\theta)}, \quad (13)$$

$$\begin{aligned} G(\theta) &= \frac{C_{66}C_{12}^2 - C_{11}C_{22}C_{66}}{D \cos^2(\theta) \sin^2(\theta) + (C_{12}^2 - C_{11}C_{22})[\cos^2(\theta) - \sin^2(\theta)]^2}, \end{aligned} \quad (14)$$

where A , B , and D are defined as $A = (C_{11}C_{22} - C_{12}^2)/C_{66} - 2C_{12}$, $B = C_{11} + C_{22} - (C_{11}C_{22} - C_{12}^2)/C_{66}$, and $D = -4C_{66}(C_{22} + C_{11} + 2C_{12})$. The mechanical performance of a material can be described by Young's moduli $Y(\theta)$, shear modulus $G(\theta)$, and Poisson's ratio $\nu(\theta)$, which have important implications for the design of flexible electronic devices. From Fig. 7, one can note that there exists evident

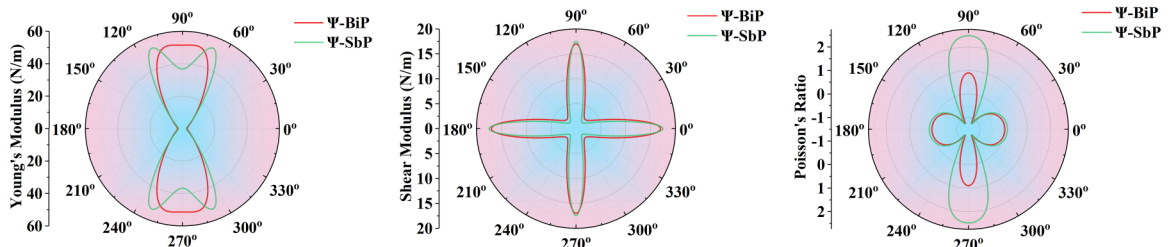


FIG. 7. Spatial-dependent mechanics of Young's modulus, shear modulus, and Poisson's ratio for ψ -BiP and ψ -SbP.

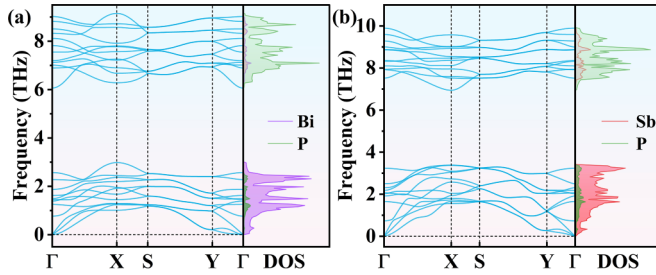


FIG. 8. Phonon dispersions and phonon density of state for (a) ψ -BiP and (b) ψ -SbP.

anisotropic behavior in the $Y(\theta)$ and $v(\theta)$ of ψ -BiP and ψ -SbP monolayers.

Figure 8 depicts the phonon dispersions of monolayer binary compounds ψ -BiP and ψ -SbP obtained from the DFPT method. Obviously, ψ -BiP and ψ -SbP are free of imaginary phonon frequencies in all phonon spectra, confirming their dynamical stability. In addition, we also calculated phonons for the most favorable phases of the considered materials (see Fig. S2 of Supplemental Material [47]). As shown in Fig. 9, AIMD simulations are utilized to further verify the thermodynamic stability of the binary compounds of ψ -BiP and ψ -SbP at 300 K. The energy of the system fluctuates only slightly as time progresses, and the inset shows snapshots at 100 ps after the simulations have concluded. It is found that ψ -BiP and ψ -SbP are less deformed and maintain their original shape. In order to quantify the deformation within a crystal structure, the four bond order parameters Q_4 , Q_6 , W_4 , and W_6 are generally sufficient, and detailed calculations are provided in Refs. [53,54]. The findings demonstrated that Q_4 , Q_6 , W_4 , and W_6 had not seen any notable alterations. Such AIMD results indicate that ψ -BiP and ψ -SbP monolayers also exhibit good thermal stability at room temperature.

IV. CONCLUSION

The crystal structure of monolayer group-V binary compounds is systematically investigated based on a random sampling strategy combined with space group and graph theory. Based on first principles, we calculate the piezoelectric properties of these allotropes with relatively low-energy α , β , γ , δ , λ , and ψ phases. The calculations show that compared with the obvious piezoelectric effect in α -SbN ($d_{11} = 118.29$ pm/V), α -SbP ($d_{11} = 142.44$ pm/V), and α -SbAs ($d_{11} =$

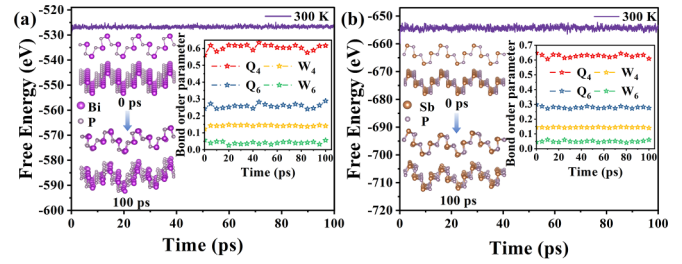


FIG. 9. AIMD simulations of the ψ -BiP and ψ -SbP monolayers at 300 K for 100 ps. The inset shows the bond order parameter during MD simulation.

243.45 pm/V) reported by Yin *et al.* [23], the d_{11} of ψ -SbP and ψ -BiP is evaluated to be as high as 263.77 and 298.48 pm/V, respectively, presenting giant piezoelectric effects. Such a superb piezoelectric performance in ψ -SbP and ψ -BiP even exceeds that previously reported in the classic piezoelectric material SnSe ($d_{11} = 250.58$ pm/V). Additionally, ψ -SbP and ψ -BiP monolayers also exhibit evident anisotropic piezoelectric responses, and the uniquely flexible structure and point-group symmetry serve as a theoretical guide in designing semiconductors with excellent piezoelectric properties. Meanwhile, the HSE06 hybrid functional-based calculation shows that both ψ -BiP and ψ -SbP are direct band-gap semiconductors with gaps of 0.91 and 0.72 eV, respectively. Finally, the Born-Huang criteria, phonon spectrum, and *ab initio* molecular dynamics simulation are utilized to verify that ψ -BiP and ψ -SbP are mechanically, dynamically, and thermally stable. The results presented in this paper shed light on the energy stability and piezoelectric effect of monolayer group-V 2D materials. ψ -BiP and ψ -SbP with a giant piezoelectric performance create different prospects for designing piezoelectric devices with superior properties.

ACKNOWLEDGMENTS

This work is supported by the National Natural Science Foundation of China (Grants No. 11974299 and No. 11974300), the Scientific Research Foundation of Education Bureau of Hunan Province (20B582, 20K127, 19C1746, and 20A503), the Youth Science and Technology Talent Project of Hunan Province (2022RC1197), the Science Fund for Distinguished Young Scholars of Hunan Province of China (No. 2021JJ10036), and the Program for Changjiang Scholars and Innovative Research Team in University (IRT13093).

- [1] L. C. Gomes, A. Carvalho, and A. H. Castro Neto, *Phys. Rev. B* **92**, 214103 (2015).
- [2] K. H. Michel and B. Verberck, *Phys. Rev. B* **80**, 224301 (2009).
- [3] W. Wu, L. Wang, Y. Li, F. Zhang, L. Lin, S. Niu, D. Chenet, X. Zhang, Y. Hao, T. F. Heinz, J. Hone, and Z. L. Wang, *Nature (London)* **514**, 470 (2014).
- [4] H. Zhu, Y. Wang, J. Xiao, M. Liu, S. Xiong, Z. J. Wong, Z. Ye, Y. Ye, X. Yin, and X. Zhang, *Nat. Nanotechnol.* **10**, 151 (2015).

- [5] A. Chandrasekaran, A. Mishra, and A. K. Singh, *Nano Lett.* **17**, 3290 (2017).
- [6] Q. Zhang, S. Zuo, P. Chen, and C. Pan, *InfoMat* **3**, 987 (2021).
- [7] C. Dagdeviren, P. Joe, O. L. Tuzman, K.-I. Park, K. J. Lee, Y. Shi, Y. Huang, and J. A. Rogers, *Extreme Mech. Lett.* **9**, 269 (2016).
- [8] A. Andrei, K. Krupa, M. Jozwik, P. Delobelle, L. Hirsinger, C. Gorecki, L. Nieradko, and C. Meunier, *Sens. Actuators, A* **141**, 565 (2008).

- [9] A. Khan, Z. Abas, H. S. Kim, and I. K. Oh, *Smart Mater. Struct.* **25**, 053002 (2016).
- [10] P. Lin, C. Pan, and Z. L. Wang, *Mater. Today Nano* **4**, 17 (2018).
- [11] F. Zhang, J. Qiu, H. Guo, L. Wu, B. Zhu, K. Zheng, H. Li, Z. Wang, X. Chen, and J. Yu, *Nanoscale* **13**, 15611 (2021).
- [12] M. N. Blonsky, H. L. Zhuang, A. K. Singh, and R. G. Hennig, *ACS Nano* **9**, 9885 (2015).
- [13] K.-A. N. Duerloo, M. T. Ong, and E. J. Reed, *J. Phys. Chem. Lett.* **3**, 2871 (2012).
- [14] C. Tan, X. Cao, X.-J. Wu, Q. He, J. Yang, X. Zhang, J. Chen, W. Zhao, S. Han, G.-H. Nam, M. Sindoro, and H. Zhang, *Chem. Rev.* **117**, 6225 (2017).
- [15] S. Guo, Y. Zhang, Y. Ge, S. Zhang, H. Zeng, and H. Zhang, *Adv. Mater.* **31**, 1902352 (2019).
- [16] J. Sturala, A. Ambrosi, Z. Sofer, and M. Pumera, *Angew. Chem., Int. Ed.* **57**, 14837 (2018).
- [17] S. Zhang, Z. Yan, Y. Li, Z. Chen, and H. Zeng, *Angew. Chem., Int. Ed.* **54**, 3112 (2015).
- [18] S. Zhang, M. Xie, F. Li, Z. Yan, Y. Li, E. Kan, W. Liu, Z. Chen, and H. Zeng, *Angew. Chem., Int. Ed.* **55**, 1666 (2016).
- [19] J. Ji, X. Song, J. Liu, Z. Yan, C. Huo, S. Zhang, M. Su, L. Liao, W. Wang, Z. Ni, Y. Hao, and H. Zeng, *Nat. Commun.* **7**, 13352 (2016).
- [20] W. Tian, S. Zhang, C. Huo, D. Zhu, Q. Li, L. Wang, X. Ren, L. Xie, S. Guo, P. K. Chu, H. Zeng, and K. Huo, *ACS Nano* **12**, 1887 (2018).
- [21] R. Gusmao, Z. Sofer, D. Bousa, and M. Pumera, *Angew. Chem., Int. Ed.* **56**, 14417 (2017).
- [22] H.-H. Sun, M.-X. Wang, F. Zhu, G.-Y. Wang, H.-Y. Ma, Z.-A. Xu, Q. Liao, Y. Lu, C.-L. Gao, Y.-Y. Li, C. Liu, D. Qian, D. Guan, and J.-F. Jia, *Nano Lett.* **17**, 3035 (2017).
- [23] H. Yin, J. Gao, G.-P. Zheng, Y. Wang, and Y. Ma, *J. Phys. Chem. C* **121**, 25576 (2017).
- [24] C. C. Xiao, F. Wang, S. Y. A. Yang, Y. H. Lu, Y. P. Feng, and S. B. Zhang, *Adv. Funct. Mater.* **28**, 1707383 (2018).
- [25] R. Fei, W. Li, J. Li, and L. Yang, *Appl. Phys. Lett.* **107**, 173104 (2015).
- [26] B. Liu, M. Kopf, A. N. Abbas, X. Wang, Q. Guo, Y. Jia, F. Xia, R. Wehrich, F. Bachhuber, F. Pielhofer, H. Wang, R. Dhall, S. B. Cronin, M. Ge, X. Fang, T. Nilges, and C. Zhou, *Adv. Mater.* **27**, 4423 (2015).
- [27] G. Kresse and J. Furthmüller, *Phys. Rev. B* **54**, 11169 (1996).
- [28] J. P. Perdew, K. Burke, and M. Ernzerhof, *Phys. Rev. Lett.* **77**, 3865 (1996).
- [29] G. Kresse and D. Joubert, *Phys. Rev. B* **59**, 1758 (1999).
- [30] P. E. Blöchl, *Phys. Rev. B* **50**, 17953 (1994).
- [31] H. J. Monkhorst and J. D. Pack, *Phys. Rev. B* **13**, 5188 (1976).
- [32] V. Wang, N. Xu, J.-C. Liu, G. Tang, and W.-T. Geng, *Comput. Phys. Commun.* **267**, 108033 (2021).
- [33] A. Togo and I. Tanaka, *Scr. Mater.* **108**, 1 (2015).
- [34] X. Wu, D. Vanderbilt, and D. R. Hamann, *Phys. Rev. B* **72**, 035105 (2005).
- [35] J. Heyd, G. E. Scuseria, and M. Ernzerhof, *J. Chem. Phys.* **118**, 8207 (2003).
- [36] W. Z. Xiao, G. Xiao, Q. Y. Rong, and L. L. Wang, *Phys. Chem. Chem. Phys.* **20**, 22027 (2018).
- [37] E. Cadelano, P. L. Palla, S. Giordano, and L. Colombo, *Phys. Rev. B* **82**, 235414 (2010).
- [38] D. Vanderbilt, *J. Phys. Chem. Solids* **61**, 147 (2000).
- [39] R. D. King-Smith and D. Vanderbilt, *Phys. Rev. B* **47**, 1651 (1993).
- [40] H. J. Jia, H. M. Mu, J. P. Li, Y. Z. Zhao, Y. X. Wu, and X. C. Wang, *Phys. Chem. Chem. Phys.* **20**, 26288 (2018).
- [41] F. Chen, H. Xu, J. Wang, Z. Wang, X. Liu, Y. Lu, and L. Wang, *J. Appl. Phys.* **125**, 214303 (2019).
- [42] W.-Z. Xiao, G. Xiao, Q.-Y. Rong, and L.-L. Wang, *Mater. Res. Express* **5**, 035903 (2018).
- [43] T. Kocabaş, D. Çakır, O. Gülseren, F. Ay, N. Kosku Perkgöz, and C. Sevik, *Nanoscale* **10**, 7803 (2018).
- [44] S. Ma, C. He, L. Z. Sun, H. Lin, Y. Li, and K. W. Zhang, *Phys. Chem. Chem. Phys.* **17**, 32009 (2015).
- [45] X. Shi, C. He, C. J. Pickard, C. Tang, and J. Zhong, *Phys. Rev. B* **97**, 014104 (2018).
- [46] W. Z. Xiao, L. Xu, G. Xiao, L. L. Wang, and X. Y. Dai, *Phys. Chem. Chem. Phys.* **22**, 14503 (2020).
- [47] See Supplemental Material at <http://link.aps.org/supplemental/10.1103/PhysRevMaterials.7.016001> for the total energies per atom of group-V binary allotrope compounds and phonon dispersions for the most favorable phases of the considered materials
- [48] M. Born and K. Huang, *Am. J. Phys.* **23**, 474 (1955).
- [49] S.-D. Guo, X.-S. Guo, Y.-Y. Zhang, and K. Luo, *J. Alloys Compd.* **822**, 153577 (2020).
- [50] M. S. Hybertsen and S. G. Louie, *Phys. Rev. Lett.* **55**, 1418 (1985).
- [51] J. Heyd, G. E. Scuseria, and M. Ernzerhof, *J. Chem. Phys.* **124**, 219906 (2006).
- [52] M. Yagmurcukardes, C. Sevik, and F. M. Peeters, *Phys. Rev. B* **100**, 045415 (2019).
- [53] W. Yanting, S. Teitel, and D. Christoph, *J. Chem. Phys.* **122**, 214722 (2005).
- [54] P. J. Steinhardt, D. R. Nelson, and M. Ronchetti, *Phys. Rev. B* **28**, 784 (1983).